OXFORD

Human Molecular Genetics, 2023, Vol. 00, 00, 1–13
https://doi.org/10.1093/hmg/ddad162
Advance access publication date 4 October 2023
Original Article

Isogenic pairs of induced-pluripotent stem-derived endothelial cells identify *DYRK1A/PPARG/EGR1* pathway is responsible for Down syndrome-associated pulmonary hypertension

Hidehiro Suginobe[1], Hidekazu Ishida[1,*], Yoichiro Ishii[2], Kazutoshi Ueda[1], Chika Yoshihara[1], Atsuko Ueyama[1], Renjie Wang[1], Hirofumi Tsuru[1,3], Kazuhisa Hashimoto[1], Masaki Hirose[1], Ryo Ishii[1], Jun Narita[1], Yasuji Kitabatake[1], Keiichi Ozono[1]

[1]Department of Pediatrics, Osaka University Graduate School of Medicine, 2-2 Yamadaoka, Suita, Osaka 565-0871, Japan
[2]Department of Pediatric Cardiology, Osaka Children's and Women's Hospital, 840 Murodohcho, Izumi, Osaka 594-1101, Japan
[3]Department of Pediatrics, Niigata University School of Medicine, 1-757 Asahimachi-dori, chuo-ku, Niigata 951-8510, Japan
*Corresponding author. Hidekazu Ishida, M.D., Ph.D., Department of Pediatrics, Osaka University Graduate School of Medicine, 22 Yamadaoka, Suita, Osaka 565-0871, Japan. Tel: +81-6-6879-3932; Fax: +81-6-6879-3939; E-mail: hideishi@ped.med.osaka-u.ac.jp

Abstract

Down syndrome (DS) is the most prevalent chromosomal disorder associated with a higher incidence of pulmonary arterial hypertension (PAH). The dysfunction of vascular endothelial cells (ECs) is known to cause pulmonary arterial remodeling in PAH, although the physiological characteristics of ECs harboring trisomy 21 (T21) are still unknown. In this study, we analyzed the human vascular ECs by utilizing the isogenic pairs of T21-induced pluripotent stem cells (iPSCs) and corrected disomy 21 (cDi21)-iPSCs. In T21-iPSC-derived ECs, apoptosis and mitochondrial reactive oxygen species (mROS) were significantly increased, and angiogenesis and oxygen consumption rate (OCR) were significantly impaired as compared with cDi21-iPSC-derived ECs. The RNA-sequencing identified that *EGR1* on chromosome 5 was significantly upregulated in T21-ECs. Both *EGR1* suppression by siRNA and pharmacological inhibitor could recover the apoptosis, mROS, angiogenesis, and OCR in T21-ECs. Alternately, the study also revealed that *DYRK1A* was responsible to increase *EGR1* expression via *PPARG* suppression, and that chemical inhibition of *DYRK1A* could restore the apoptosis, mROS, angiogenesis, and OCR in T21-ECs. Finally, we demonstrated that *EGR1* was significantly upregulated in the pulmonary arterial ECs from lung specimens of a patient with DS and PAH. In conclusion, *DYRK1A/PPARG/EGR1* pathway could play a central role for the pulmonary EC functions and thus be associated with the pathogenesis of PAH in DS.

Graphical Abstract

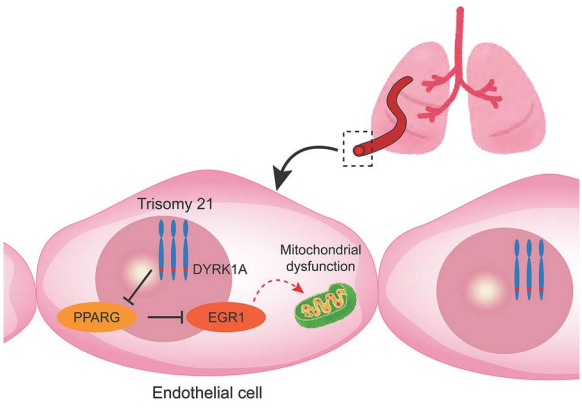

Keywords: induced pluripotent stem cell; Down syndrome; endothelial cell; EGR1; pulmonary hypertension

Received: June 26, 2022. **Revised:** August 30, 2023. **Accepted:** August 30, 2023.

Introduction

Down syndrome (DS) caused by the trisomy of human chromosome 21 (T21) is the most frequent chromosomal disorder with an estimated prevalence of one in every 700 births each year [1]. It has been known that DS is associated with a higher incidence of pulmonary arterial hypertension (PAH), especially in patients with congenital heart defects [2, 3]. A recent large cohort study revealed that the prevalence of PAH in DS was estimated at 28%, far higher than in general population [4]. The major risk factors associated with PAH in DS have been linked to respiratory diseases such as upper airway obstruction, hypoventilation, and recurrent respiratory infections [5]. However, the pulmonary histology showed that early progression of pulmonary arterial remodeling could occur in patients with DS [6, 7]. Previous studies regarding the pathogenesis of idiopathic or hereditary PAH (I/HPAH) demonstrated that pulmonary vascular remodeling was involved in the vascular endothelial cell (EC) dysfunction [8, 9]. In contrast, the cellular characteristics and behaviors of vascular ECs with T21 were not elucidated till present, mainly due to the lack of appropriate cellular and animal models for DS that harbor a complete T21.

Recently, patient-specific induced pluripotent stem cells (iPSCs) became a useful technique for exploring the cellular and molecular pathogeneses of various genetic disorders. In this context, Gu *et al.* reported that iPSC-derived ECs from patients with HPAH and *BMPR2* gene mutation showed a significant EC dysfunction, consequently, a specific molecular pathway for the protection of EC functions was identified [10]. This study suggested that iPSC-derived ECs could be a reliable method for the investigation of the molecular pathogenesis of PAH, despite the incomplete illustration of the pulmonary or systemic arterial ECs in iPSC-derived ECs.

In this study, we mainly utilized the isogenic pairs of human iPSC-derived ECs which were established by patients with DS and the genetically corrected disomy 21 (cDi21) line to investigate the cellular physiology of ECs harboring T21.

Results

All lines of human iPSCs established from patients with DS and healthy controls can efficiently differentiate into ECs

We used MiraCell iPS Cell to Endothelial Cell Differentiation Kit for the differentiation of our iPSC lines into vascular ECs. EC morphology showed a typical cobblestone appearance, similar in T21-, T21'-, cDi21-, and two healthy controls-iPSC-derived ECs (HC_1 and HC_2). We confirmed that almost all cells were CD31-positive ECs by immunocytochemistry, and we estimated the purity of ECs by flow cytometry for CD31 as 97.3 ± 1.4%, 97.2 ± 0.97%, 98.7 ± 0.54%, 92.4 ± 3.4%, and 97.1 ± 0.082%, respectively (Supplementary Fig. 1).

The ECs differentiated from cDi21-iPSCs show equivalent cellular physiological functions as those from healthy control-iPSCs

In order to exclude the possible inter-individual errors of iPSC lines, we generated the isogenic pairs of T21-iPSCs and cDi21-iPSCs [11]. Before comparing cellular functions of ECs between the isogenic pairs of iPSC-derived ECs, we confirmed that ECs, derived from cDi21-iPSCs harboring experimentally corrected normal karyotype, were physiologically equivalent to those derived from HC-iPSCs. In this framework, we carried out the following five fundamental cellular functional assays: cellular proliferation, migration, adhesion, apoptosis, and angiogenesis. We did not find a significant difference among the vascular ECs differentiated from cDi21-iPSCs and the two independent lines of HC-iPSCs (Supplementary Fig. 2). Therefore, cDi21-ECs could be considered as an isogenic normal control of T21-ECs hereafter.

T21-ECs show increased apoptosis, impaired angiogenesis, and mitochondrial dysfunction

Afterwards, we compared cellular physiological functions between the vascular ECs derived from isogenic pairs of T21- and cDi21-iPSCs, and another DS patient derived (T21')-iPSCs. No significant difference was detected among T21-, T21'-, and cDi21-ECs in the properties of proliferation (cDi21, 23.8 ± 2.99%; T21, 23.6 ± 1.74%; T21', 23.7 ± 2.17%; $P = 0.997$; Fig. 1A), migration (cDi21, 1.00 ± 0.076; T21, 0.96 ± 0.079; T21', 0.96 ± 0.038; $P = 0.872$; Fig. 1B), and adhesion (cDi21, 560.2 ± 40.08/mm^2; T21, 416.0 ± 68.70/mm^2; T21', 506.4 ± 52.57/mm^2; $P = 0.251$; Fig. 1C). In contrast, T21- and T21'-ECs exhibited significantly more apoptotic cells as assessed by flow cytometry for annexin V and propidium iodide (cDi21, 1.85 ± 0.287%; T21, 6.65 ± 0.794%; T21', 7.41 ± 0.248%; $P < 0.01$ vs cDi21; Fig. 1, D and E). Alternately, we analyzed angiogenesis abilities by tube formation assay, and found that T21- and T21'-ECs were significantly impaired in angiogenesis (cDi21, 114.8 ± 4.52; T21, 44.67 ± 4.26; T21', 48.5 ± 3.25; $P < 0.001$ vs cDi21; Fig. 1, F and G).

Assuming that mitochondrial dysfunction is involved in cellular apoptosis, we investigated mitochondrial respiratory activity, and found that T21- and T21'-ECs exhibited higher production of mitochondrial reactive oxygen species (mROS) as compared with cDi21-ECs (cDi21, 142.0 ± 1.25; T21, 240.1 ± 22.1; T21', 209.6 ± 14.3; $P < 0.05$ vs cDi21; Fig. 1, H and I). Next, we evaluated mitochondrial respiratory function by oxygen consumption rate (OCR) assay. In this context, T21- and T21'-ECs showed a significant decrease in normalized rate where basal respiration and maximal respiration were significantly impaired (basal: cDi21, 100.0 ± 3.34; T21, 51.8 ± 10.31; T21', 42.1 ± 0.045; $P < 0.01$ vs cDi21; maximal: cDi21, 200.0 ± 20.19; T21, 89.72 ± 15.53; T21', 79.34 ± 11.81; $P < 0.01$ vs cDi21; Fig. 1, J and K). Consequently, DS specific ECs were more apoptotic and less angiogenic compared with cDi21-ECs, which could be linked to the mitochondrial respiratory dysfunction and oxidative stress. These results regarding cellular features of DS-ECs are consistent with the previous reports using pulmonary ECs-derived from patients with I/HPAH [12–14].

RNA-sequencing shows that gene expression profiles are altered in T21-ECs and identifies *EGR1* as a candidate for mitochondrial dysfunction in DS

To clarify the molecular mechanisms that underlie T21-EC dysfunctions, we carried out an RNA-sequencing analysis using two independent iPSC-derived EC lines of patients with DS (T21 and T21'), two independent iPSC-derived EC lines of HC_1 and HC_2, and an isogenic iPSC-derived EC line of cDi21. T-distributed stochastic neighbor embedding (tSNE) showed distinctive expression patterns among each of the two lines of T21-ECs, as well as the two lines of HC-ECs and cDi21-ECs. Noting that, the expression pattern of cDi21-ECs was similar to HC-ECs (Fig. 2A). The pathway analyses demonstrated that both the mitochondria related genes and endothelial cell related genes were dysregulated in T21-ECs (Fig. 2, B and C). To identify the causative genes of T21-EC mitochondrial and endothelial

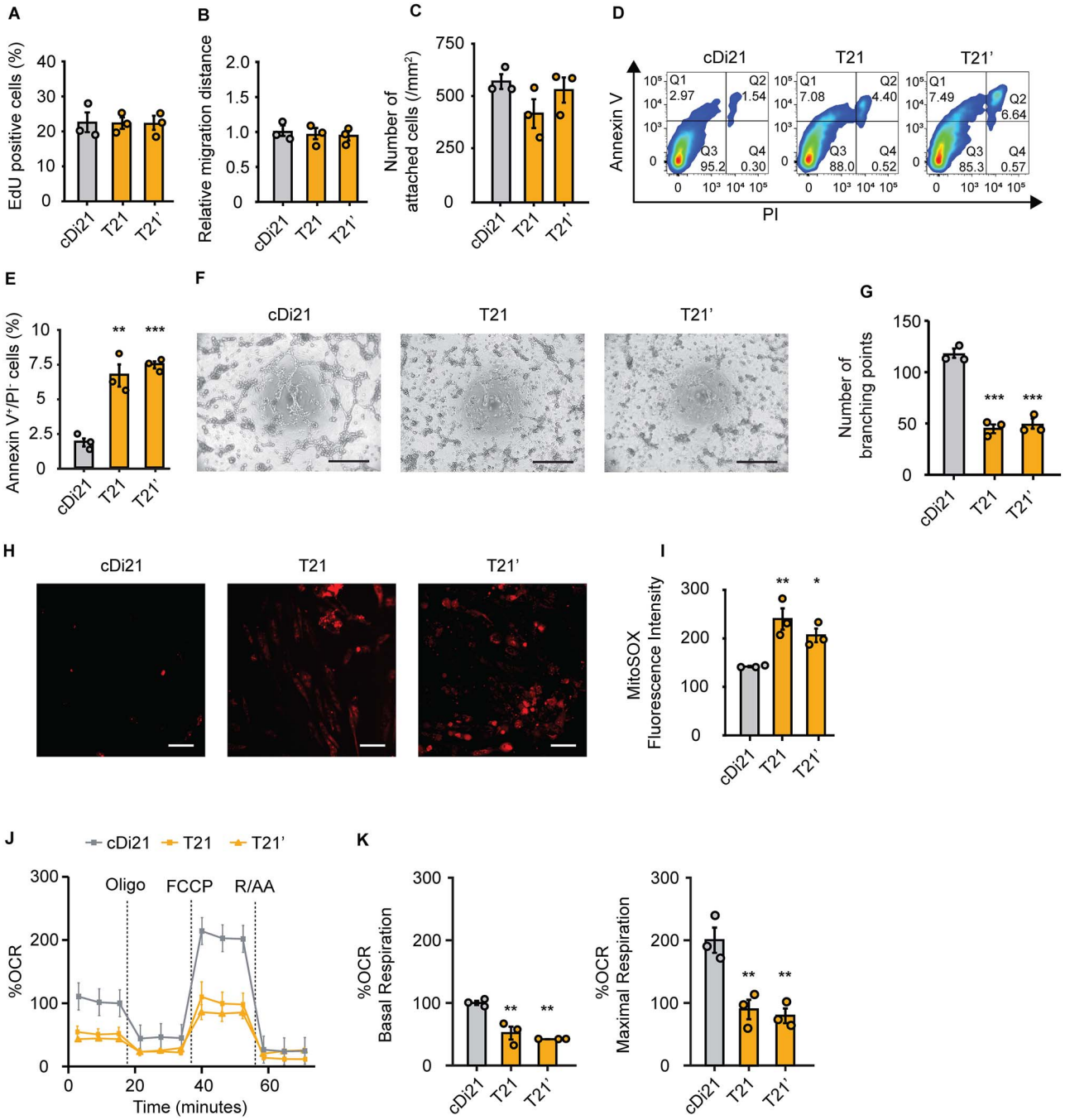

Figure 1. Cellular physiology and mitochondrial respiratory function of T21-ECs and cDi21-ECs. (A) Proliferation assay evaluating the percentages of EdU-positive cells. There is no significant difference among cDi21-, T21-, and T21'-ECs. (B) Relative migration distance 12 h after the wound scratch of the cells. There is no significant difference among cDi21-, T21-, and T21'-ECs. (C) Cell adhesion assay by counting the number of attached cells 2 h after seeding. There is no significant difference among cDi21-, T21-, and T21'-ECs. (D) Representative images of apoptosis assay by flow cytometry for annexin V and propidium iodide (PI). (E) The quantitative analyses of annexin V-positive and PI-negative cell populations show that apoptotic cells are significantly increased in T21- and T21'-ECs as compared with cDi21-ECs. (F) Representative images of phase contrast microscopy in tube formation assay. Note that lots of cellular tubes are formed in cDi21-ECs. Scale bar: 500 μm. (G) The quantitative assessments tube formation show that ability of angiogenesis is impaired in T21- and T21'-ECs as compared with cDi21-ECs. (H) Representative fluorescent images of MitoSOX red staining for mitochondrial superoxide production assay. Scale bar: 50 μm. (I) The quantitative measurements of MitoSOX fluorescence intensity show that mitochondrial superoxide production is significantly increased in T21- and T21'-ECs. (J) Oxygen consumption rate (OCR) at baseline and after sequential injection of oligomycin, carbonyl cyanide 4-(trifluoromethoxy) phenylhydrazone (FCCP), and Rotenone/Antimycin A (R/AA). (K) Basal respiration and maximal respiration are significantly impaired in T21- and T21'-ECs. Three independent experiments were conducted each in A, B, C, E, G, and I. Five independent experiments were conducted in J and K. Data are presented as mean ± SEM. Data were analyzed by the Tukey–Kramer multiple comparison test. $^{***}P < 0.001$, $^{**}P < 0.01$, $^{*}P < 0.05$ as compared to cDi21-ECs.

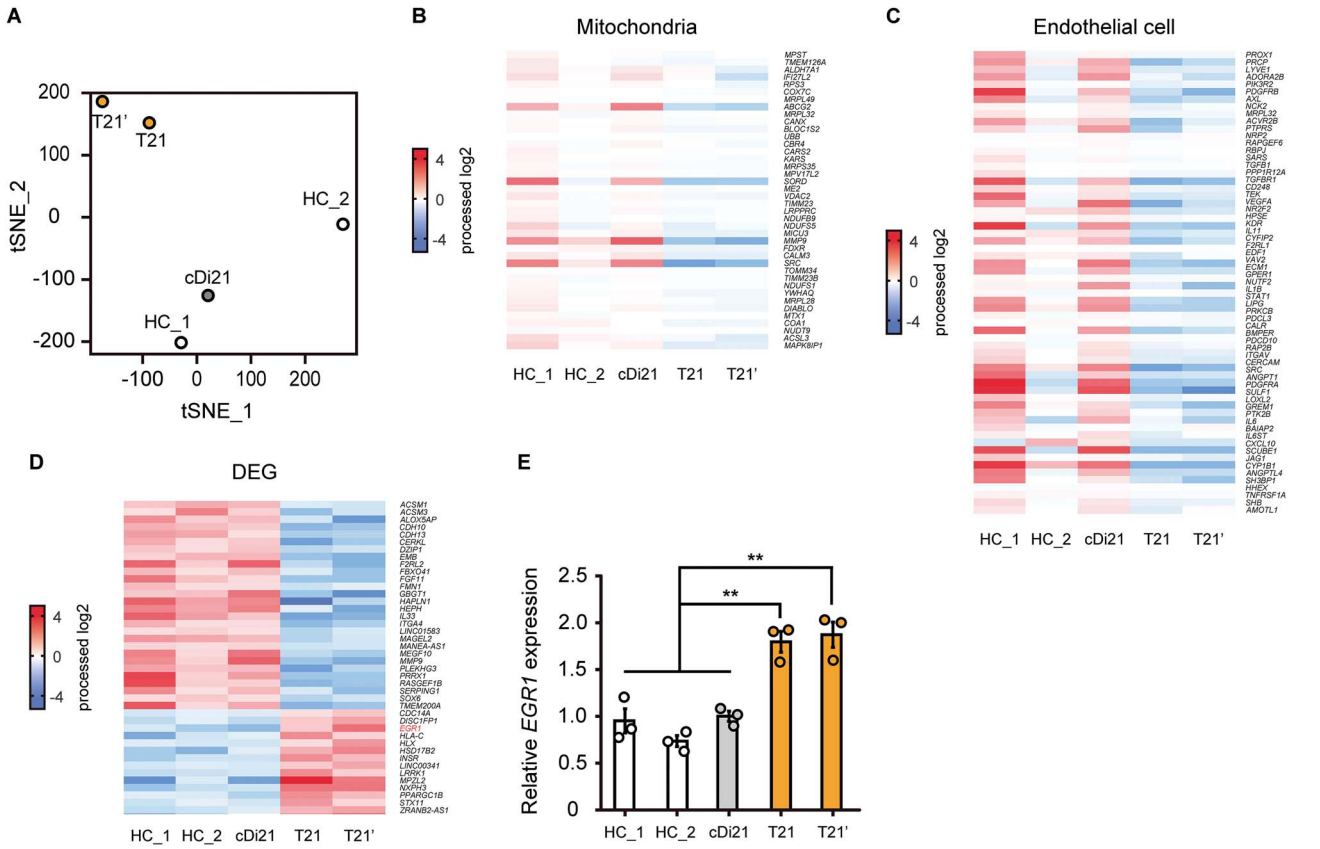

Figure 2. The RNA-sequencing analyses of T21-, cDi21-, and healthy control-ECs. RNAs were extracted from two independent iPSC-derived EC lines of patients with Down syndrome (T21 and T21'), two independent iPSC-derived EC lines of healthy controls (HC_1 and HC_2), and an isogenic iPSC-derived EC line of corrected to disomy 21 (cDi21). (A) T-distributed stochastic neighbor embedding (tSNE) plots of RNA-sequencing. The comprehensive expression patterns of T21- and T21'-ECs are separated from cDi21-ECs and HC-ECs. (B) The pathway analysis of RNA-sequencing reveals that the mitochondria related genes are dysregulated in T21- and T21'-ECs as compared to HC-ECs and cDi21-ECs. (C) The RNA-sequencing reveals that the endothelial cell related genes are dysregulated in T21- and T21'-ECs. (D) Differential gene expression (DEG) analysis reveals significantly upregulated and downregulated genes in T21-ECs. (E) Quantitative PCR analysis of *EGR1* in T21-, T21'-, cDi21-, and HC-ECs. Data are presented as mean ± SEM. Data were analyzed using the Tukey–Kramer multiple comparison test. $^{**}P < 0.01$.

dysfunction, we focused on the differential expression genes among T21- and control-lines of ECs. As a result, we identified significantly upregulated and downregulated genes, where none was located on the chromosome 21 (Fig. 2D). Furthermore, we searched for candidate genes which could result in EC dysfunctions associated with PAH, apoptosis, and mitochondrial dysfunction, and found *EGR1* as a potent candidate for T21-EC dysfunction. Our results confirmed that *EGR1* expression was significantly increased approximately 1.9-fold in both T21-ECs and T21'-ECs compared to cDi21-ECs by quantitative polymerase chain reaction (PCR) analysis (Fig. 2E). Noting that, EGR1, which is a transcriptional factor encoded on chromosome 5, is known to promote apoptosis via mitochondria-dependent manner [15]. In addition, EGR1 is reported to be involved in the vascular remodeling of PAH [16].

Suppression of *EGR1* expression restores angiogenesis and mitochondrial dysfunctions of T21-ECs

To determine whether the increase in *EGR1* expression is truly responsible for endothelial and mitochondrial dysfunctions of T21-ECs, we analyzed angiogenesis and OCR subsequently after si*EGR1* treatment. First, we checked the suppression of *EGR1* expression in T21-ECs following the treatment of two different targets of si*EGR1*; both could effectively reduce *EGR1* expression in T21- ECs (Supplementary Fig. 3A). As the 24 h treatment of lipofection reagent disturbed the cellular viability and angiogenesis of iPSC-derived ECs, we selected 6 h treatment of si*EGR1*. We confirmed *EGR1* expression levels in T21-, T21'-, cDi21-, and HC-ECs under 6 h treatment of si*EGR1*, and found that the relative mRNA expressions of *EGR1* in all lines were suppressed at similar levels. Although *EGR1* expression level is known to rapidly change depending on the cellular status, we confirmed that suppression of *EGR1* expression was persistent for at least 6 h after the retrieval of si*EGR1* from culture media, meaning that there was no time effect during the angiogenesis and OCR experimental assays (Supplementary Fig. 3B). Afterward, we found that the reduction of *EGR1* expression could significantly restore the angiogenesis property, mitochondrial OCR, the ratio of apoptotic cells, and mROS production both in T21- and T21'-ECs (Fig. 3), suggesting that the elevation of *EGR1* expression could be substantially responsible for DS-associate endothelial and mitochondrial dysfunctions.

Next, to confirm whether *EGR1* suppression by the chemical inhibitor was also effective to restore the T21-EC dysfunction, we administered pioglitazone to the culture media of T21-, T21'- and cDi21-ECs. Pioglitazone is a PPARγ activator that reduces *EGR1* expression [17]. Alternatively, we confirmed that a supplementation of 10 μM pioglitazone could efficiently increase *PPARG* expression and reduce *EGR1* expression in T21-ECs (Fig. 4, A and B). Therefore, we clearly verified that angiogenesis

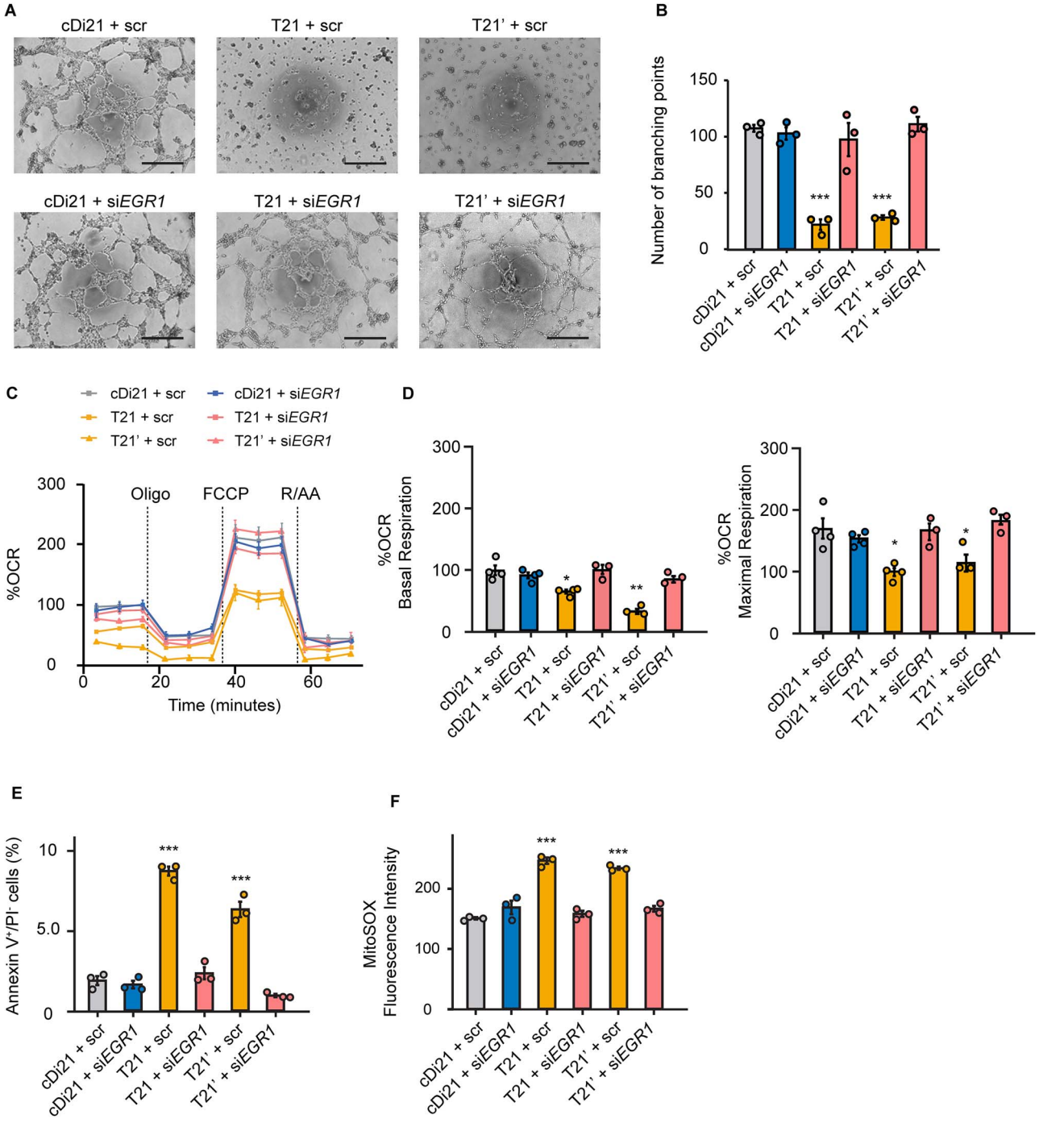

Figure 3. Knockdown of *EGR1* expression in T21-EC restores angiogenesis and mitochondrial respiratory function. (A) Representative phase contrast images of tube formation assay in scrambled siRNA-treated or si*EGR1*-treated ECs. Scale bar: 500 μm. (B) The quantitative analyses of tube formation assays reveal that angiogenesis is significantly recovered in si*EGR1* treated T21- and T21'-ECs as same level as that of cDi21-ECs. (C) OCR of each cell line and condition at baseline and after sequential supplementation of oligomycin (Oligo), FCCP, and Rotenone/Antimycin A (R/AA). (D) Quantitative analyses of basal respiration and maximal respiration show significant improvement of OCR in si*EGR1* treated T21- and T21'-ECs. (E) Quantitative analyses of annexin V-positive and PI-negative cell populations show that apoptotic cells are significantly decreased in si*EGR1*-treated T21- and T21'-ECs, similar to cDi21-ECs. (F) Quantitative measurements of MitoSOX fluorescence intensity show that the level of mitochondrial superoxide production is significantly recovered in si*EGR1*-treated T21- and T21'-ECs, which is similar to the level in cDi21-ECs.Three to four independent experiments were conducted in each. Data are presented as mean ± SEM. Data were analyzed by Tukey–Kramer multiple comparison test. ***$P < 0.001$, **$P < 0.01$, *$P < 0.05$.

property, mitochondrial OCR, the ratio of apoptotic cells, and mROS production could be significantly recovered in T21- and T21'-ECs after pioglitazone treatment (Fig. 4, C–H). This result suggested that pioglitazone could be a candidate for drug treatment to improve the endothelial function in patients with DS.

Chemical inhibition of DYRK1A can modulate *PPARG* and *EGR1* expressions leading to recovery of EC function in DS

In order to investigate how *EGR1* expression is altered in T21-ECs, we examined the candidates of responsible genes on chromosome 21. *DYRK1A* is located within the DS critical region of

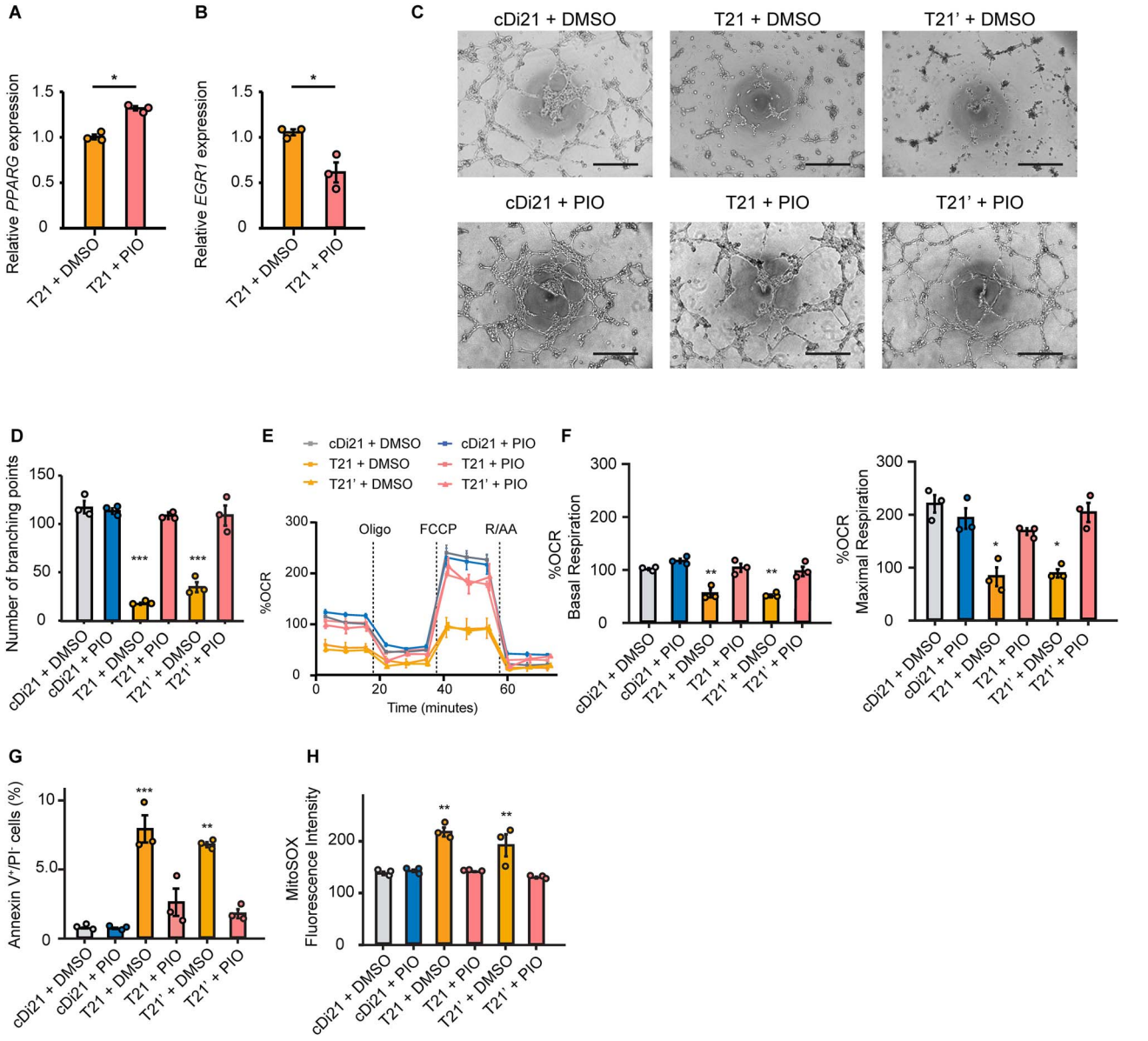

Figure 4. Pioglitazone suppresses *EGR1* mRNA expression in DS-ECs and can restore angiogenesis and mitochondrial respiratory function. (A and B) Relative mRNA expression of *PPARG* and *EGR1* in T21-ECs treated with DMSO or pioglitazone (PIO). PIO treatment significantly increases *PPARG* expression and suppresses *EGR1* expression. (C) Representative phase contrast images of tube formation assays in each cell line and condition. Scale bar: 500 μm. (D) The quantitative analyses of tube formation assays demonstrate that angiogenesis is significantly recovered in PIO-treated T21- and T21'-ECs as same level as that of cDi21-ECs. (E) OCR of each cell line and condition at baseline and after sequential treatment of oligomycin (Oligo), FCCP, and Rotenone/Antimycin A (R/AA). (F) Quantitative analyses of basal respiration and maximal respiration show significant improvement of OCR in PIO-treated T21- and T21'-ECs. (G) Quantitative analyses of annexin V-positive and PI-negative cell populations show that apoptotic cells are significantly decreased in PIO-treated T21- and T21'-ECs, similar to cDi21-ECs. (H) Quantitative measurements of MitoSOX fluorescence intensity show that the level of mitochondrial superoxide production is significantly restored in pioglitazone-treated T21- and T21'-ECs, which is similar to the level in cDi21-ECs. Three independent experiments were conducted in each. Data are presented as mean ± SEM. Data were analyzed by unpaired *t*-test and Tukey–Kramer multiple comparison test. ***$P < 0.001$, **$P < 0.01$, *$P < 0.05$.

the chromosome 21, and any elevation in its expression is reported to impair the angiogenesis, which is related to the suppression of solid tumor growth in DS through ECs inactivation [18]. Moreover, overexpression of *DYRK1A* was reported to suppress *PPARG* expression [19]. Given that *PPARG* was reported to inhibit *EGR1* expression [20], we hypothesized that an upregulation of *DYRK1A* might increase *EGR1* expression via suppressing *PPARG* pathway in T21-ECs. On the other side, to examine whether *DYRK1A* was responsible for the endothelial dysfunction in DS, we administered harmine, a potent *DYRK1A* inhibitor, to the culture media of T21-, T21'-, and cDi21-ECs. Consequently, we confirmed that *DYRK1A* expression level was almost 1.5-fold higher in our T21- and T21'-ECs by RNA-sequencing and quantitative PCR analyses (Fig. 5A). Harmine treatment could effectively increase *PPARG* expression and suppress *EGR1* expression in T21- and T21'-ECs with similar levels of cDi21-ECs (Fig. 5, B and C). Therefore, we demonstrated that harmine treatment could significantly improve the angiogenesis property, the mitochondrial respiratory function, apoptosis, and mROS production in T21- and T21'-ECs (Fig. 5, D–I).

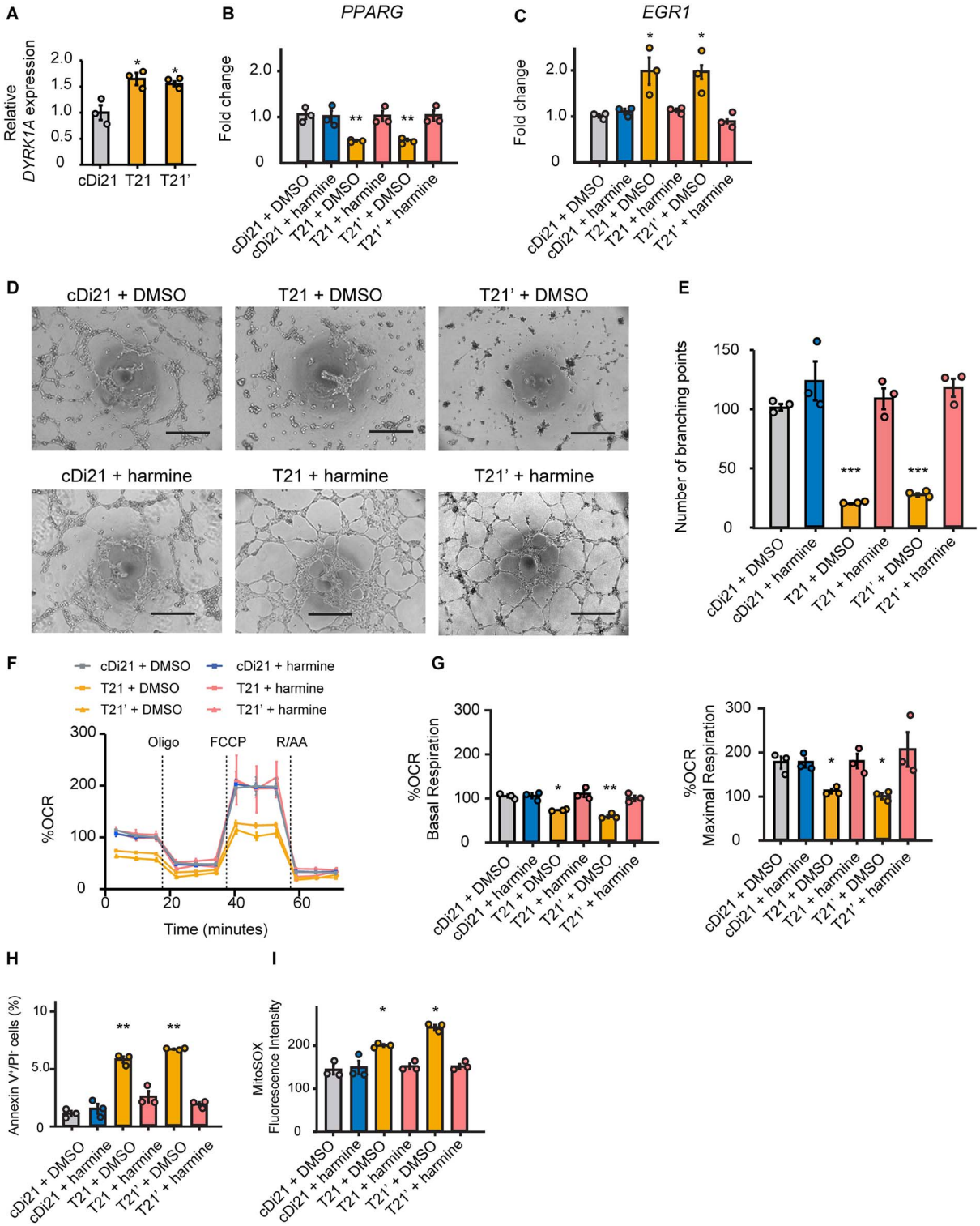

Figure 5. DYRK1A inhibitor, harmine reduces *EGR1* mRNA expression in T21-EC via *PPARG* pathway and restores angiogenesis and mitochondrial respiratory function. (A) Relative mRNA expressions of *DYRK1A* in T21- and T21'-ECs, evaluated by quantitative PCR. Approximately 1.5-fold higher expression is observed both in T21- and T21'-ECs as compared with cDi21-ECs. (B) Relative mRNA expression of *PPARG* in cDi21-ECs, T21-, and T21'-ECs treated with DMSO or harmine; the latter significantly increases *PPARG* expression in T21- and T21'-ECs, but not in cDi21-ECs. (C) Relative mRNA expression of *EGR1* treated with DMSO or harmine; the latter significantly reduces *EGR1* expression in T21- and T21'-ECs. (D) Representative phase contrast images of tube formation assays in each cell line and condition. Scale bar: 500 μm. (E) Quantitative analyses of tube formation assays reveal that angiogenesis is significantly recovered in harmine-treated T21- and T21'-ECs as same level as that of cDi21-ECs. (F) OCR of each cell line and condition at baseline and after sequential treatment of oligomycin (Oligo), FCCP, and Rotenone/Antimycin A (R/AA). (G) Quantitative analyses of basal respiration and maximal respiration show significant improvement of OCR in harmine-treated T21- and T21'-ECs. (H) Quantitative analyses of annexin V-positive and PI-negative cell populations show that apoptotic cells are significantly decreased in harmine-treated T21- and T21'-ECs, similar to cDi21-ECs. (I) Quantitative measurements of MitoSOX fluorescence intensity show that the level of mitochondrial superoxide production is significantly decreased in harmine-treated T21- and T21'-ECs, which is similar to the level in cDi21-ECs. Three to four independent experiments were conducted in each. Data are presented as mean ± SEM. Data were analyzed by Tukey–Kramer multiple comparison test. ***$P < 0.001$, **$P < 0.01$, *$P < 0.05$.

DYRK1A overexpression deteriorates endothelial and mitochondrial function in control ECs

We transfected a vector expressing *DYRK1A* into cDi21-ECs and two healthy control (HC)-ECs to investigate whether *DYRK1A* is solely responsible for endothelial and mitochondrial dysfunctions in DS-ECs. First, we examined the relative expression levels of *DYRK1A* in cDi21-ECs. Additionally, we found that *DYRK1A* is 20-fold more abundant in *DYRK1A* expression vector-cDi21- than in empty vector (EV) transfected-cDi21-ECs (Fig. 6A). *DYRK1A* overexpression significantly downregulated and upregulated the expression of *PPARG* and *EGR1*, respectively (Fig. 6A). *DYRK1A* overexpression impaired tube formation abilities and OCR in cDi21- and HC-ECs (Fig. 6, B–E). Then, the experiment revealed significant apoptosis of ECs and increased mROS levels in *DYRK1A*-overexpressed-cDi21- and HC-ECs (Fig. 6, F and G). Overall, our results suggest that *DYRK1A* upregulation could affect the expression levels of *PPARG* and *EGR1* in DS-ECs, leading to EC dysfunction in patients with DS.

EGR1 is upregulated in the pulmonary ECs of a human patient with DS and PAH

Finally, to evaluate whether EGR1 plays an important role in the pathogenesis of PAH in human patients with DS, we analyzed the lung specimens of a patient with DS and PAH, whose upper lobe of his left lung was partly resected due to a massive hemoptysis with severe PAH subsequent to a cardiac surgery for a ventricular septal defect. Therefore, we conducted an immunohistochemistry of EGR1 in the lung tissues and counted the percentages of EGR1-positive nuclei of his pulmonary arterial ECs (Fig. 7, A and B). The quantitative analysis showed that the number of EGR1- positive pulmonary arterial ECs was significantly greater as compared with a healthy control (healthy control, $21.5 \pm 4.37\%$; Down syndrome, $81.5 \pm 3.89\%$; $P < 0.001$; Fig. 7C). This outcome suggested that EGR1 is upregulated in human patients with DS and PAH, indicating that EGR1 is a key regulator of pulmonary EC dysfunction in DS as well as in iPSC-derived ECs.

Discussion

In this study, we originally proved that vascular EC function is impaired in DS by using isogenic pairs of iPSCs derived from DS patients. Recently, patient-specific iPSC technology facilitates the investigation of pathogenic mechanisms in many genetic disorders including PAH. Nevertheless, to reduce the inter-individual error of iPSC lines, isogenic pairs of iPSCs have been considered as an appropriate in *in vitro* model [21, 22].

First of all, we analyzed the five cellular physiological functions of T21-ECs, including proliferation, adhesion, migration, apoptosis, and angiogenesis abilities. According to previous studies utilizing the ECs from patients with I/HPAH or animal models, these cellular properties were impaired in PAH [23, 24]. In fact, we demonstrated that T21-ECs had an impaired angiogenesis and an increased apoptosis, which is compatible with the previous studies of IPAH both *in vitro* and *in vivo* [25]. In contrast, we could not find any significant difference in cellular proliferation, migration, and adhesion in T21-ECs, although many previous studies revealed that the latter properties of cellular function were impaired in pulmonary ECs of PAH [23]. This discrepancy might be due to the difference of pathogenesis between I/H-PAH and PAH associated with DS. Afterward, we focused on the mitochondrial respiratory function of T21-ECs as mitochondrial dysfunction was reported in DS; a previous study proved that fetal dermal fibroblasts from patients with DS exhibited the impairment of mitochondrial respiration and elevation of ROS [26]. On the other hand, the impairment of mitochondrial respiratory function and metabolism have been thoroughly examined in patients with PAH and model animals [12–14, 24]. Several studies showed that ROS increased in the lung tissues of patients with PAH [12], and that OCR of pulmonary ECs in patients with IPAH significantly decreased [24]. Although we were unable to assess the metabolic shift of glycolysis and alteration of mitochondrial membrane potential, our results suggest that mitochondrial dysfunction could be associated with the pathogenesis of PAH in DS.

Subsequently, we found that the comprehensive gene expression patterns in T21-ECs changed compared with healthy control-ECs. In addition, we identified *EGR1* as a candidate gene for mitochondrial dysfunction in DS. EGR1, which is a Cys2-His2 type zinc finger transcription factor, resides on human chromosome 5 [27]. Its expression is induced by various stimuli including hypoxia, shear stress, and pro-inflammatory cytokines [28–30]. EGR1 binds to GC-rich domain of genes such as *TGFB* [31], *PDGFA* [29], *PDGFB* [32], and *p53* [33], all of which are involved in the pathogenesis of PAH in animal models and human patients [34–36]. Additionally, EGR1 is also involved in the mitochondrial function [15, 37]. Later, we showed that treatment with si*EGR1* and pioglitazone could restore the mitochondrial function and angiogenesis in DS-ECs, suggesting that EGR1 is a key regulator of the mitochondrial function and plays an important role in PAH pathogenesis of patients with DS.

Next, we focused on *DYRK1A* and *PPARG* pathways. *DYRK1A* is one of the most important genes in human chromosome 21, which is closely associated with the pathogenesis of DS mainly in neurological disorders [38]. *Dyrk1a* transgenic mouse was reported to decrease *PPARG* expression, and *PPARG* was described as an important upstream regulator of *EGR1* [17, 19]. Moreover, *PPARG* pathway has attracted attention for its involvement in the pathogenesis of PAH [39, 40]. We demonstrated that a chemical inhibition of *DYRK1A* could restore the mitochondrial function and angiogenesis in T21-ECs. On the contrary, *DYRK1A* overexpression might deteriorate the mitochondrial and endothelial functions in control ECs. Taken together, we strongly suggest that *DYRK1A/PPARG/EGR1* pathway would play a central role in the pathogenesis of PAH associated with DS.

Finally, to confirm whether our *in vitro* experiments using patient-specific iPSC lines truly recapitulate the pathogenesis of PAH in DS, we analyzed the lung specimen of a patient with DS with severe PAH and congenital heart disease; the results showed that EGR1 expression in the pulmonary arterial ECs was significantly elevated in the patient with DS with PAH, which indicates that EGR1 is a potent key regulator of the pathogenesis of PAH in human patients with DS, and that the *DYRK1A/PPARG/EGR1* pathway might be a candidate therapeutic target of DS with PAH.

Nevertheless, there are several limitations in this study; the most important one is that the differentiated ECs from iPSCs are not specific to pulmonary ECs. However, a previous study using iPSCs from patients with HPAH and a *BMPR2* mutation could also successfully recapitulate the pathological phenotype of EC dysfunction [10]. Another limitation resides on the number of patients in both *in vitro* and *in vivo* experiments. We cannot exclude the possibility of inter-individual variability. We utilized the isogenic pairs of iPSCs: T21- and cDi21-iPSCs; therefore, we considered that the possible errors of iPSC lines could be reduced in this study. Moreover, we analyzed the lung specimen from only one patient with DS, due to the fact that human lung specimens from patients with DS are hard to obtain. Since *EGR1* expression is

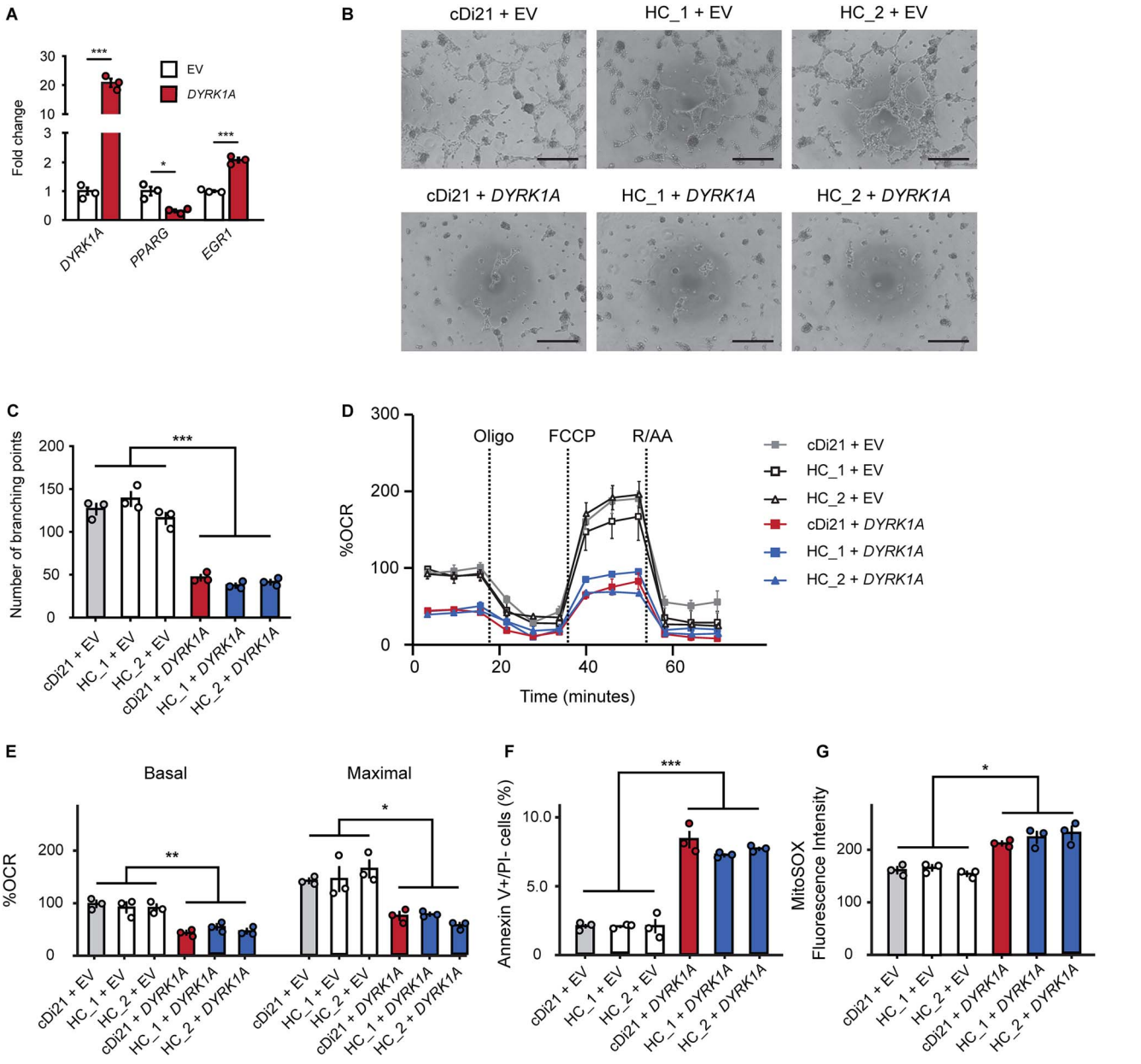

Figure 6. ***DYRK1A* overexpression impairs angiogenesis and mitochondrial respiratory function in cDi21- and HC-ECs**. (A) Transfection of the *DYRK1A*-expression vector induced significant higher mRNA level of *DYRK1A* in cDi21-ECs as compared with that of empty vector (EV). Overexpression of *DYRK1A* results in a significant decrease of *PPARG* and an increase of *EGR1* levels in cDi21-ECs compared with EV-treated-ECs. (B) Representative images of the tube formation assays in cDi21- and two HC-EC lines treated with EV and *DYRK1A* expression vector, visualized by phase contrast microscopy. Scale bar: 500 μm. (C) Quantitative analyses of the tube formation assays show that angiogenesis is significantly impaired in *DYRK1A*-overexpressed cDi21- and HC-ECs. (D) OCR at baseline and after sequential treatment of oligomycin (Oligo), FCCP, and Rotenone/Antimycin A (R/AA) in each line treated with EV and *DRYK1A* expression vector. (E) Quantitative analyses of basal respiration and maximal respiration show significant impairment of OCR in cells treated with *DYRK1A*-expression vector. (F) Quantitative analyses of annexin V-positive and PI-negative cell populations demonstrate that the proportion of apoptotic cells significantly increased in *DYRK1A*-overexpressed ECs. (G) Quantitative measurements of MitoSOX fluorescence intensity show a significant increase in the level of mitochondrial superoxide production in *DYRK1A*-overexpressed ECs. Three independent experiments were conducted in each. Data are presented as mean ± SEM. Data were analyzed by unpaired *t*-test and Tukey–Kramer multiple comparison test. ***$P < 0.001$, **$P < 0.01$, *$P < 0.05$.

associated with cell shear stress, we assessed the response of T21-ECs to shear stress using a liquid flow pump system. However, T21- and T21'-ECs detached from the cell culture plates even under weak stimuli (2 to 5 dyne). Therefore, we could not determine the shear stress response of these cells *in vitro*. Consequently, further studies are necessary to reveal whether the suppression of EGR1 is effective for DS-associated PAH in human.

In conclusion, we identified EGR1 as a key regulator of mitochondrial dysfunction of pulmonary ECs in DS. Moreover, we suggested that *DYRK1A/PPARG/EGR1* could be a central pathway for pulmonary EC dysfunction in patients with DS.

Materials and Methods

Generation and culture of iPSCs from patients with DS and healthy controls

T21-iPSC lines were generated as previously described [11, 41]. Briefly, the dermal fibroblasts cultured from two patients with DS

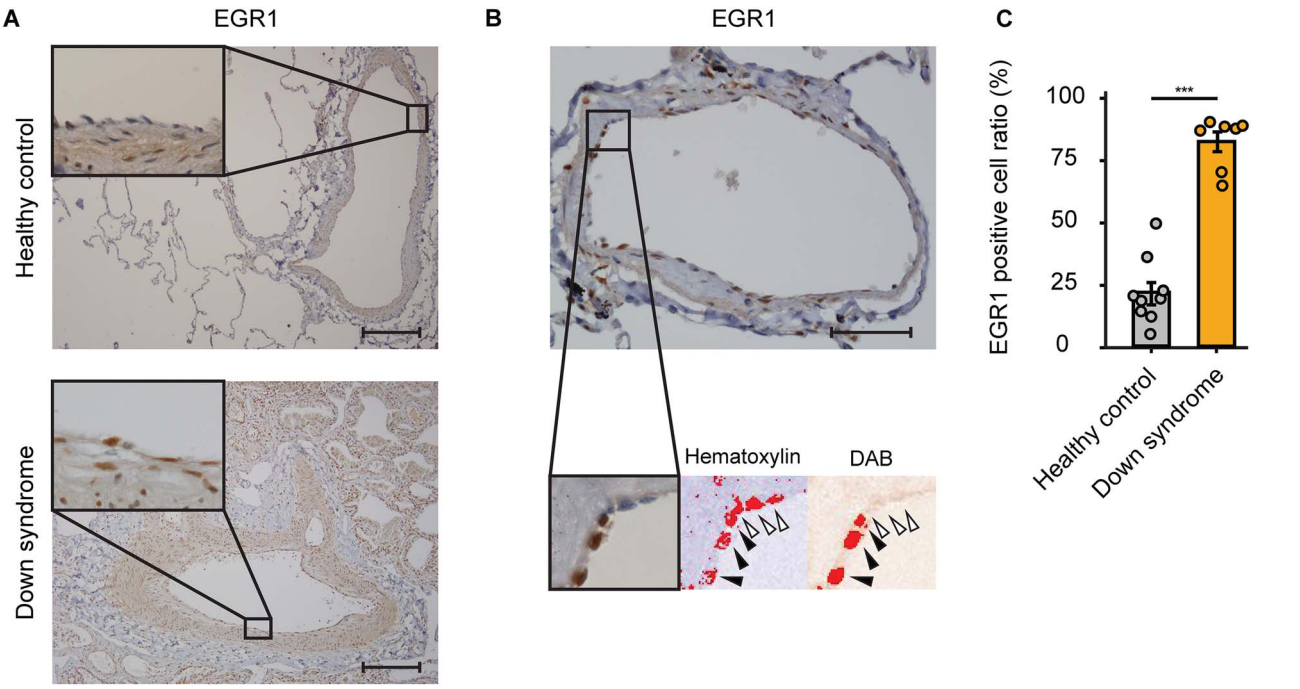

Figure 7. Immunohistochemistry of EGR1 in pulmonary arteries of patients with Down syndrome and PAH. (A) Representative images of immunohistochemistry of EGR1 in the lung tissues of healthy control (upper panels) and patients with DS and PAH (lower panels). Scale bar: 200 μm. (B) Representative images of quantitative evaluation for EGR1 positive pulmonary ECs. The parentages of 3,3′-Diaminobenzidine (DAB) positive nuclei of pulmonary arterial ECs were counted. The black arrowheads indicate EGR1-positive nuclei and the white arrowhead indicates EGR1-negative nucleus. Scale bar: 50 μm. (C) EGR1-positive cell ratio of pulmonary ECs in DS is significantly higher than that of healthy control. Seven arteries and nine arteries were analyzed in healthy control and in DS, respectively. Data are presented as mean ± SEM. Data were analyzed by an unpaired Student's *t* test. ***$P < 0.001$.

and two healthy infants were transfected by a Sendai virus vector encoding human *OCT3/4*, *SOX2*, *KLF4*, and *CMYC*. Noting that, no patient with DS had congenital heart disease. We generated a cDi21-iPSC line by introducing a chromosome elimination cassette into the extra maternal chromosome by TALENs, obtained after Cre-loxP mediated recombination and FIAU selection [11]. The iPSC lines were characterized by immunostaining for pluripotency markers, karyotyping, and teratoma formation. We maintained the cells by Cellartis DEF-CS 500 Basal Medium (Takara bio, Kusatsu, Japan) and passaged following the manufacturer's recommendations.

Differentiation to vascular ECs

We differentiated ECs from each iPSC line by using MiraCell iPS Cell to Endothelial Cell Differentiation Kit (Takara bio) following the manufacturer's protocol, and maintained on fibronectin-coated cell-culture dishes with MiraCell EC Culture Medium (Takara bio). ECs were used for all experiments between passages 2 and 6.

Immunofluorescence and flow cytometry analyses

For immunocytochemical analysis, we fixed the cells with 4% paraformaldehyde for 10 min, and permeabilized it with a PBS solution containing 0.1% of Triton-X 100 for 10 min. After blocking with 5% FBS, we incubated the cells with anti-CD31 (1/30; 14-0319-82, Thermo Fisher Scientific, Waltham, MA, USA) primary antibody at 4°C overnight. Afterward, we incubated the cells with secondary Goat anti-Mouse Alexa Fluor 488 antibody (1/400; A-11001, Thermo Fisher Scientific) for 60 min at room temperature, and we stained the nuclei with Hoechst 33 342 (H342, Dojindo Molecular Technologies, Kumamoto, Japan). We developed the images by IN Cell Analyzer 6000 (GE Healthcare, Chicago, IL, USA). For flow cytometry, we suspended the cells in HBSS containing 3% FBS and 0.3 mM EDTA, fixed with 4% paraformaldehyde, and stained with the same antibodies used in immunofluorescence. Mouse IgG isotype control (401 401, BioLegend, San Diego, CA, USA) was applied as a negative control. We analyzed the cells via a BD FACS Canto II (BD Biosciences, Franklin Lakes, NJ, USA), and performed the data analysis using FlowJo v10 software (BD Biosciences).

Proliferation assay

We cultured ECs at 15 000 cells per well in 96-well plates for one day, then, we applied 10 μM EdU (Click-iT EdU Cell Proliferation Kit for Imaging, Thermo Fisher Scientific) and incubated the plates for 24 h. Afterward, we stained the cells with AlexaFluor 488 (Thermo Fisher Scientific) and the nuclei with Hoechst 33 342. We analyzed the cells at a × 400 magnification by IN Cell Analyzer 6000, and we calculated the percentages of EdU-positive nuclei.

Apoptosis assay

Prior to the apoptosis assay, we cultured the cells at 100 000 cells per well in 6-well plates for 24 h. Next, we washed the cells with Cell Staining Buffer (Biolegend) and stained them with FITC-Annexin V and propidium iodide (PI) (Biolegend) at 4°C for 10 min, and analyzed them by BD FACS Canto II. Data analysis was performed using FlowJo v10 software.

Migration assay

We modified the migration assay from the previous publication [42]; we cultured the cells at 60 000 per well in 24-well plates 24 h

prior to the assay. After confirming the confluence, we scratched the cells with a vertical wound through the cell monolayer using a 200 μl pipette tip. We washed the cellular debris with PBS twice and added MiraCell EC Culture Medium to the cells. We obtained the phase contrast microscopic images and measured the distance of one side to the other side of the wound. We analyzed the ratio of shortening from the start to 12 h compared with a control using ImageJ software (https://imagej.nih.gov/ij/index.html).

Adhesion assay

We seeded the cells at 20 000 cells per well in 96-well plates coated with fibronectin. Later, after 2 h incubation at 37°C, we washed the cells twice with PBS and stained them with Hoechst 33 342. We analyzed the number of nuclei by IN Cell Analyzer 6000.

Tube formation assay

We modified the tube formation assay from the previous publication [43]; we merged growth factor reduced Matrigel (Merck Millipore, Burlington, MA, USA) into 96-well plates (40 μl/well) and incubated them at 37°C for 30 min. We seeded the cells at 15 000 per well for 6 h. We captured the images with a BZ-X700 microscope (Keyence, Osaka, Japan). We quantified the tube formation by the number of branching points.

Measurement of mitochondrial reactive oxygen species (mROS)

We measured mROS using MitoSOX red (Thermo Fisher Scientific) following the manufacture's protocol. We seeded the cells briefly at 15 000 per well in 96-well black plates. We loaded the cells with 5 μM MitoSOX red and 50 nM MitoTracker Green (Thermo Fisher Scientific) for 15 min, washed twice in PBS, and analyzed them by IN Cell Analyzer 6000. We indexed the level of mROS by mean red fluorescence intensity on the mitochondria stained in green.

Measurement of OCR

We measured OCR via a Seahorse XFe96 Analyzer (Agilent Technologies, Santa Clara, CA, USA). We seeded the cells at 10 000 cells per well in 96 well Seahorse assay plates coated with fibronectin. We studied the cells in Seahorse XF DMEM (Agilent Technologies) supplemented with 10 mM glucose, 2 mM glutamine and 1 mM pyruvate. We determined OCR in the basal state or after sequentially adding 1.0 μM oligomycin, 2.0 μM carbonyl cyanide 4-(trifluoromethoxy) phenylhydrazone (FCCP), and 0.5 μM rotenone/antimycin A. We corrected the values of the OCR measurement for cell numbers and expressed the data as a percentage of the basal OCR of control cell lines.

RNA isolation and RNA-sequence

We extracted total RNA using NucleoSpin (Takara Bio) following the manufacturer's procedure; we measured the RNA concentration by NanoDrop 2000c (Thermo Fisher Scientific), and conducted an RNA-sequencing by next generation sequencer as previously described [44]. Sequencing was performed on an Illumina HiSeq 2500 platform in 75-base single-end mode (Illumina, San Diego, CA, USA). The transcriptomes of T21-ECs, healthy-ECs, and cDi21-ECs were analyzed with Subio platform (https://www.subioplatform.com/ja/). All sequence data sets are available at Gene Expression Omnibus, GSE203257.

siRNA gene silencing

Knockdown of *EGR1* was carried out using Silencer Select siRNA with Lipofectamine RNAiMAX (Thermo Fisher Scientific) following the manufacturer's protocol. Before performing tube formation assay and measuring OCR, we transfected ECs with siRNA (5 nM) for 6 h. The sequences of siRNAs were as follows; si*EGR1*_1 sense: 5′-CAACGACAGCAGUCCCAUUtt-3′, antisense: 5′-AAUGGGACUGCUGUCGUUGga-3′; si*EGR1*_2 sense: 5′-GCAGAGUCUUUUCCU GACAtt-3′, antisense: 5′-UGUCAGGAAAA GACUCUGCgg-3′.

Plasmid transfection

The plasmids pRP-Vec (pRP[Exp]-EGFP-CAG > ORF_Stuffer, Cat. VB900122-4426sjs) and pRP-DYRK1A (pRP[Exp]-EGFP-CAG > hDYRK1A[NM_001396.5], Cat. VB900135-9088zng) were purchased from VectorBuilder (Chicago, IL, USA). Differentiated ECs were transfected with the plasmids for 6 h using Lipofectamine 2000 reagent (Thermo Fisher Scientific). Subsequently, the medium was replaced with MiraCell EC Culture Medium overnight. ECs were provided for all experiments 24 h following the plasmid transfection.

Quantitative real-time PCR

We extracted total RNA using NucleoSpin RNA column kit (Takara Bio). After RNA isolation, we performed reverse transcription through the use of ReverTra ACE (TOYOBO, Osaka, Japan) following the manufacturer's instructions. Afterward, we conducted quantitative real-time PCR with QuantStudio 7 system by using THUDERBIRD SYBR qPCR Mix kit (TOYOBO). We analyzed each sample in technical triplicates with the following protocol: 10 min at 95°C, followed by 40 cycles of 15 s at 95°C, and 1 min at 60°C. Each PCR analysis was completed by a melt curve cycle of 15 s at 95°C, 60 s at 60°C, and 15 s at 95°C. We analyzed all the data by using the standard curve method, and evaluated the relative amount of mRNAs compared to that of the house-keeping gene *ACTB*. We calculated the cycle threshold under the default settings by real-time sequence detection software (Applied Biosystems).

We used the following primer pairs for qPCR; *EGR1* forward: 5′-AGCAGCACCTTCAACCCTCAGG-3′, reverse 5′-GAGTGGTTTGGCT GGGGTAACT-3′; *PPARG* forward: 5′-TGGTGACTTTATGGAGCCCAA-3′, reverse 5′-GGCAAACAGCTGTGAGGACTCAG-3′; *DYRK1A* forward: 5′-CCTTGCCATTGATATGTGGTCCC-3′, reverse 5′-GCAGGT GGAATACCCAGAACTTC-3′; *ACTB* forward: 5′-TCAAGATCATTGC TCCTCCTGAG-3′, reverse 5′-ACATCTGCTGGAAGGTGGACA-3′.

Chemical inhibition of *DYRK1A/PPARG/EGR1* pathway

We seeded the cells at 80 000 per well in 24-well plates for RNA extraction, at 100 000 per well in 6-well plates for tube formation assay, and 10 000 per well in 96 well Seahorse assay plates coated with fibronectin for OCR measurement, 24 h prior to drug treatment. We applied a 24 h treatment with 10 μM of pioglitazone (Wako, Osaka, Japan) and 2.5 μM of harmine (Thermo Fisher Scientific) for inhibiting *EGR1* and *DYRK1A*, respectively.

Immunohistochemistry for EGR1 in the lungs of a patient with DS

We performed immunohistochemistry using ImmPRESS HRP Horse Anti-Rabbit IgG PLUS Polymer Kit (Vector Laboratories, Burlingame, CA, USA) according to the manufacturer's instructions. We deparaffinized the paraffin-embedded slides in xylene and rehydrated them in a graded series of ethanol. We performed antigen retrieval by autoclaving the slides in 10 mM citrate buffer, at pH 6.0. We blocked the activity of the endogenous peroxidase with 3% hydrogen peroxide for 30 min. After blocking, we incubated the slides with a 1:200 dilution

of rabbit monoclonal anti–EGR1 antibody (ab194357, Abcam, Cambridge, UK) at 4°C overnight in a humidified chamber. Next, we incubated the slides with ImmPRESS HRP horse anti-rabbit IgG polymer reagent (Vector Laboratories) for 30 min, followed by 3,3′-diaminobenzidine (DAB) staining for 40 s. We counterstained the slides with Mayer hematoxylin, dehydrated in a graded series of ethanol followed by xylene, and mounted with Mount Quick (Daido Sangyo, Saitama, Japan). Paraffin-embedded normal lung sections were purchased from Novus Biologicals (62-years old, male, NBP2-30182).

Data availability

The RNA-sequencing raw fastq files, gene by cell transcript counts matrix, and metadata files were available in Gene Expression Omnibus database (GSE203257).

Statistics

All data were expressed as means ± standard error. We performed all statistical analyses through R version 4.0.4 and RStudio 1.4.1106. We used an unpaired *t*-test for comparison of two groups, and performed a multiple group comparison by Tukey–Kramer test. P value < 0.05 was considered to indicate a statistical significance.

Study approval

All studies using iPSCs and human lung samples are approved by the Ethics Committee of Osaka University Graduate School of Medicine (approval no. 13123-823 and no. 15118-4). Written informed consents were obtained from the parents of the patients prior to participation.

Supplementary data

Supplementary data is available at *HMG Journal* online.

Conflict of interest statement: None declared.

Funding

This study was supported by grants from the Ministry of Education, Science, Sports, and Culture of Japan [no. 17K16261 and 20K16854].

Author contributions

H.S, K.U., C.Y., A.U., R.W., H.T., conducted the cell culture and differentiation, and contributed to all experimental measurements. H.I., R.I., J.N., K.O. designed all the study. K.H. and M.H. corrected the sample of the patients and controls. H.S. and Y.I. analyzed the RNA-sequence data. Y.K. established the T21- and cDi21-, and healthy-iPSC lines. H.S. and H.I. wrote the manuscript. H.I., Y.K., K.O. revised the data and the manuscript. All authors approved the final version of the manuscript.

References

1. Presson AP, Partyka G, Jensen KM. *et al.* Current estimate of Down syndrome population prevalence in the United States. *J Pediatr* 2013;**163**:1163–8.
2. Hals J, Hagemo PS, Thaulow E. *et al.* Pulmonary vascular resistance in complete atrioventricular septal defect. A comparison between children with and without Down's syndrome. *Acta Paediatr* 1993;**82**:595–8.
3. Colvin KL, Yeager ME. What people with Down syndrome can teach us about cardiopulmonary disease. *Eur Respir Rev* 2017;**26**:160098.
4. Bush D, Galambos C, Ivy DD. *et al.* Clinical characteristics and risk factors for developing pulmonary hypertension in children with Down syndrome. *J Pediatr* 2018;**202**:212–219.e2.
5. Bush D, Galambos C, Dunbar Ivy D. Pulmonary hypertension in children with Down syndrome. *Pediatr Pulmonol* 2021;**56**:621–9.
6. Suzuki K, Yamaki S, Mimori S. *et al.* Pulmonary vascular disease in Down's syndrome with complete atrioventricular septal defect. *Am J Cardiol* 2000;**86**:434–7.
7. Clapp S, Perry BL, Farooki ZQ. *et al.* Down's syndrome, complete atrioventricular canal, and pulmonary vascular obstructive disease. *J Thorac Cardiovasc Surg* 1990;**100**:115–21.
8. Tuder RM, Archer SL, Dorfmüller P. *et al.* Relevant issues in the pathology and pathobiology of pulmonary hypertension. *J Am Coll Cardiol* 2013;**62**:D4–12.
9. Leopold JA, Maron BA. Molecular mechanisms of pulmonary vascular remodeling in pulmonary arterial hypertension. *Int J Mol Sci* 2016;**17**:761.
10. Gu M, Shao N-Y, Sa S. *et al.* Patient-specific iPSC-derived endothelial cells uncover pathways that protect against pulmonary hypertension in BMPR2 mutation carriers. *Cell Stem Cell* 2017;**20**:490–504.e5.
11. Omori S, Tanabe H, Banno K. *et al.* A pair of maternal chromosomes derived from meiotic nondisjunction in trisomy 21 affects nuclear architecture and transcriptional regulation. *Sci Rep* 2017;**7**:764.
12. Bowers R, Cool C, Murphy RC. *et al.* Oxidative stress in severe pulmonary hypertension. *Am J Respir Crit Care Med* 2004;**169**:764–9.
13. Dorfmüller P, Chaumais M-C, Giannakouli M. *et al.* Increased oxidative stress and severe arterial remodeling induced by permanent high-flow challenge in experimental pulmonary hypertension. *Respir Res* 2011;**12**:119.
14. Wedgwood S, Black SM. Role of reactive oxygen species in vascular remodeling associated with pulmonary hypertension. *Antioxid Redox Signal* 2003;**5**:759–69.
15. Yuan S, Wen J, Cheng J. *et al.* Age-associated up-regulation of EGR1 promotes granulosa cell apoptosis during follicle atresia in mice through the NF-κB pathway. *Cell Cycle* 2016;**15**:2895–905.
16. van der Feen DE, Dickinson MG, Bartelds B. *et al.* Egr-1 identifies neointimal remodeling and relates to progression in human pulmonary arterial hypertension. *J Heart Lung Transplant* 2016;**35**:481–90.
17. Wan H, Yuan Y, Liu J. *et al.* Pioglitazone, a PPAR-γ activator, attenuates the severity of cerulein-induced acute pancreatitis by modulating early growth response-1 transcription factor. *Transl Res* 2012;**160**:153–61.
18. Baek K-H, Zaslavsky A, Lynch RC. *et al.* Down's syndrome suppression of tumour growth and the role of the calcineurin inhibitor DSCR1. *Nature* 2009;**459**:1126–30.
19. Song W-J, Song E-AC, Jung M-S. *et al.* Phosphorylation and inactivation of glycogen synthase kinase 3β (GSK3β) by dual-specificity tyrosine phosphorylation-regulated kinase 1A (Dyrk1A). *J Biol Chem* 2015;**290**:2321–33.
20. Yan C, Chen J, Ding Y. *et al.* The crucial role of PPARγ-Egr-1-pro-inflammatory mediators Axis in IgG immune complex-induced acute lung injury. *Front Immunol* 2021;**12**:634889.
21. Soldner F, Laganière J, Cheng AW. *et al.* Generation of isogenic pluripotent stem cells differing exclusively at two early onset Parkinson point mutations. *Cell* 2011;**146**:318–31.

22. Kim HS, Bernitz JM, Lee D-F. *et al.* Genomic editing tools to model human diseases with isogenic pluripotent stem cells. *Stem Cells Dev* 2014;**23**:2673–86.
23. Humbert M, Guignabert C, Bonnet S. *et al.* Pathology and pathobiology of pulmonary hypertension: state of the art and research perspectives. *Eur Respir J* 2019;**53**:1801887.
24. Xu W, Koeck T, Lara AR. *et al.* Alterations of cellular bioenergetics in pulmonary artery endothelial cells. *Proc Natl Acad Sci U S A* 2007;**104**:1342–7.
25. Xu W, Erzurum SC. Endothelial cell energy metabolism, proliferation, and apoptosis in pulmonary hypertension. *Compr Physiol* 2011;**1**:357–72.
26. Izzo A, Mollo N, Nitti M. *et al.* Mitochondrial dysfunction in Down syndrome: molecular mechanisms and therapeutic targets. *Mol Med* 2018;**24**:2.
27. Thiel G, Cibelli G. Regulation of life and death by the zinc finger transcription factor Egr-1. *J Cell Physiol* 2002;**193**:287–92.
28. Lo LW, Cheng JJ, Chiu JJ. *et al.* Endothelial exposure to hypoxia induces Egr-1 expression involving PKCalpha-mediated Ras/Raf-1/ERK1/2 pathway. *J Cell Physiol* 2001;**188**:304–12.
29. Khachigian LM, Anderson KR, Halnon NJ. *et al.* Egr-1 is activated in endothelial cells exposed to fluid shear stress and interacts with a novel shear-stress-response element in the PDGF A-chain promoter. *Arterioscler Thromb Vasc Biol* 1997;**17**:2280–6.
30. Goetze S, Kintscher U, Kaneshiro K. *et al.* TNFalpha induces expression of transcription factors c-fos, Egr-1, and Ets-1 in vascular lesions through extracellular signal-regulated kinases 1/2. *Atherosclerosis* 2001;**159**:93–101.
31. Baron V, Adamson ED, Calogero A. *et al.* The transcription factor Egr1 is a direct regulator of multiple tumor suppressors including TGFbeta1, PTEN, p53, and fibronectin. *Cancer Gene Ther* 2006;**13**:115–24.
32. Khachigian LM, Lindner V, Williams AJ. *et al.* Egr-1-induced endothelial gene expression: a common theme in vascular injury. *Science* 1996;**271**:1427–31.
33. Boone DN, Qi Y, Li Z. *et al.* Egr1 mediates p53-independent c-Myc-induced apoptosis via a noncanonical ARF-dependent transcriptional mechanism. *Proc Natl Acad Sci U S A* 2011;**108**:632–7.
34. Botney MD, Bahadori L, Gold LI. Vascular remodeling in primary pulmonary hypertension. Potential role for transforming growth factor-beta. *Am J Pathol* 1994;**144**:286–95.
35. Perros F, Montani D, Dorfmüller P. *et al.* Platelet-derived growth factor expression and function in idiopathic pulmonary arterial hypertension. *Am J Respir Crit Care Med* 2008;**178**:81–8.
36. Wang Z, Yang K, Zheng Q. *et al.* Divergent changes of p53 in pulmonary arterial endothelial and smooth muscle cells involved in the development of pulmonary hypertension. *Am J Physiol Lung Cell Mol Physiol* 2019;**316**:L216–28.
37. Nemani N, Dong Z, Daw CC. *et al.* Mitochondrial pyruvate and fatty acid flux modulate MICU1-dependent control of MCU activity. *Sci Signal* 2020;**13**:eaaz6206.
38. Duchon A, Herault Y. DYRK1A, a dosage-sensitive gene involved in neurodevelopmental disorders, is a target for drug development in Down syndrome. *Front Behav Neurosci* 2016;**10**:104.
39. Ameshima S, Golpon H, Cool CD. *et al.* Peroxisome proliferator-activated receptor gamma (PPARgamma) expression is decreased in pulmonary hypertension and affects endothelial cell growth. *Circ Res* 2003;**92**:1162–9.
40. Hansmann G, Wagner RA, Schellong S. *et al.* Pulmonary arterial hypertension is linked to insulin resistance and reversed by peroxisome proliferator-activated receptor-gamma activation. *Circulation* 2007;**115**:1275–84.
41. Banno K, Omori S, Hirata K. *et al.* Systematic cellular disease models reveal synergistic interaction of trisomy 21 and GATA1 mutations in hematopoietic abnormalities. *Cell Rep* 2016;**15**:1228–41.
42. Liang C-C, Park AY, Guan J-L. In vitro scratch assay: a convenient and inexpensive method for analysis of cell migration in vitro. *Nat Protoc* 2007;**2**:329–33.
43. Arnaoutova I, Kleinman HK. In vitro angiogenesis: endothelial cell tube formation on gelled basement membrane extract. *Nat Protoc* 2010;**5**:628–35.
44. Tsuru H, Ishida H, Narita J. *et al.* Cardiac fibroblasts play pathogenic roles in idiopathic restrictive cardiomyopathy. *Circ J* 2021;**85**:677–86.